Light-Induced Covalent Immobilization of Monolayers of Magnetic Nanoparticles on Hydrogen-Terminated Silicon

Gyu Leem,[†] Shishan Zhang,[†] Andrew C. Jamison,[†] Eduard Galstyan,[‡] Irene Rusakova,[‡] Bernd Lorenz,[‡] Dmitri Litvinov,[§] and T. Randall Lee*[,†,‡]

Departments of Chemistry and Chemical Engineering, Texas Center for Superconductivity, and Center for Nanomagnetic Systems, University of Houston, 4800 Calhoun Road, Houston, Texas 77204

ABSTRACT Specifically tailored ω-alkenyl-1-carboxylic acids were synthesized for use as surfactants in the single-step preparation of manganese ferrite ($MnFe_2O_4$) nanoparticles (NPs). Monodisperse manganese ferrite NPs terminated with ω-alkenyl moieties were prepared via a one-pot reaction at high temperature without the need of ligand exchange. Using this approach, simple adjustment of the rate of heating allowed precise tuning of the size of the nanoparticles, which were characterized in bulk form by transmission electron microscopy (TEM), Fourier-transform infrared (FT-IR) spectroscopy, and X-ray diffraction (XRD). These surfactant-coated magnetic nanoparticles were then deposited onto hydrogen-terminated silicon(111) wafers and covalently anchored to the surface by UV-initiated covalent bonding. Analysis by scanning electron microscopy (SEM) and X-ray photoelectron spectroscopy (XPS) confirmed that the UV treatment led to covalent immobilization of the NPs on the silicon surface with a consistent packing density across the surface. The magnetic properties of the stable, surface-bound nanoparticle arrays were characterized using a superconducting quantum interference device (SQUID) magnetometer. The materials and methods described here are being developed for use in bit-patterned ultrahigh density magnetic recording media and nanoscale biomagnetic sensing.

KEYWORDS: UV-induced covalent attachment • magnetic nanoparticle arrays • silicon substrates • bit-patterned magnetic recording media

INTRODUCTION

The synthesis, characterization, and manipulation of magnetic nanoparticles (NPs) have been driven by their potential use in ultrahigh density data storage (1−4), ferrofluid technology (5), medical drug delivery (6−8), and magnetic resonance imaging (MRI) (9, 10). For these applications, chemical synthesis techniques have been widely used because of their ability to produce the targeted nanoparticles in sufficient quantities (11). Synthetic methods that have been applied to magnetic NP preparation include reverse micelle (12, 13), thermal decomposition (14−16), and solid-phase reactions (17). For highly sensitive magnetic and biomedical applications, magnetic NPs with a uniform size are needed to ensure the success of such applications and to optimize their potential (14). For example, monodisperse $MnFe_2O_4$ nanoparticles with narrow size distributions have been generated using a "hot" organometallic synthesis route (14, 15). These NPs were prepared via a thermal decomposition reaction involving the reduction of organometallic reagents in the presence of a long chain 1,2-diol, oleic acid, and oleylamine.

For certain device applications, it is necessary that the magnetic NPs be anchored in an ordered fashion on an appropriate substrate, such as silicon (18). Chemical assembly and immobilization of NPs can be controlled by the introduction of capping materials onto the NP surface (19−22). Moreover, strong bonds between the NPs and an ideal substrate can be formed via bifunctional organic molecules used as surface linkers, providing a convenient assembly method to develop such NP architectures. For example, iron oxide NPs covered with initial stabilizing ligands have been modified with α,ω-heterobifunctional molecules (e.g., 10-undecenoic acid and trimethoxy-7-octen-1-yl-silane) using a ligand-exchange reaction (21, 22). These NPs, coated with unsaturated hydrocarbons, were anchored onto a hydrogen-terminated silicon surface during a thermal hydrosilylation reaction. The conventional method reports that a silicon wafer be immersed in an NP solution and heated to high temperature (e.g., 180 °C) for a period of several hours for the attachment of the NPs to the hydrogen-terminated silicon wafer (21).

Methods that are commonly used to generate organic-linked monolayers on silicon substrates include thermal hydrosilylation (23), photochemical reactions (24−30), Grignard reactions (31, 32), and electrochemical reactions (33, 34). It is worth noting that the photochemical hydrosilylation reaction offers mild reaction conditions, which can lead to high-quality monolayers that are more stable than those formed on other commonly used substrates (e.g., gold or SiO_2), where the monolayers degrade over time (29, 35, 36).

* To whom correspondence should be addressed. E-mail: trlee@uh.edu.
Received for review May 24, 2010 and accepted August 17, 2010
[†] Departments of Chemistry and Chemical Engineering, University of Houston.
[‡] Texas Center for Superconductivity, University of Houston.
[§] Center for Nanomagnetic Systems, University of Houston.
DOI: 10.1021/am100457v

Scheme 1. Preparation of Vinyl-Terminated $MnFe_2O_4$ NPs and Their Immobilization on a Hydrogen-Terminated Silicon(111) Substrate

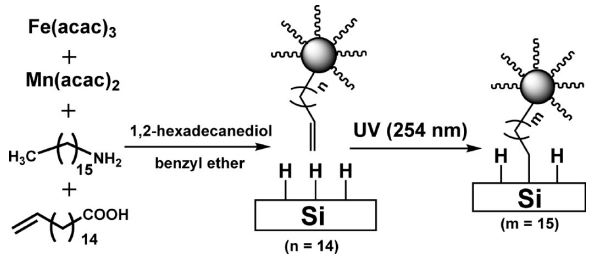

Given the enhanced stability of the C−Si bonds formed via hydrosilylation, this technique is attractive for use in applications that target high-density memory storage or magnetic nanoparticle-based biosensing. With these goals in mind, we recently communicated the UV-initiated covalent immobilization of ordered arrays of monodisperse $MnFe_2O_4$ nanoparticles on silicon wafers (37). While limited in scope, these studies provided the foundation from which to develop both a new and versatile nanoparticle synthesis methodology and a simple, mild, and efficient technique for preparing covalently anchored magnetic nanoparticle arrays that are amenable to routine photolithographic patterning.

We report here the direct preparation of size-tunable monodisperse ω-alkene-terminated $MnFe_2O_4$ nanoparticles using a one-pot reaction involving an easily deliverable custom-tailored α,ω-heterobifunctional surfactant that circumvents the need for any post-synthesis ligand exchange reactions. Specifically, we employ the thermal decomposition of selected ratios of Mn(II) and Fe(III) acetylacetonate complexes in the presence of 16-heptadecenoic acid, hexadecylamine, and 1,2-hexadecanediol to prepare monodisperse vinyl-terminated $MnFe_2O_4$ nanoparticles. Once prepared and characterized, we use UV irradiation to anchor covalently the $MnFe_2O_4$ nanoparticles to the surface of hydrogen-terminated silicon (see Scheme 1). We then evaluate the magnetic properties of the resultant highly stable magnetic NP arrays.

EXPERIMENTAL SECTION

Materials. All reactions were performed under an atmosphere of argon using standard oxygen-free conditions. Benzyl ether (99%), 1,2-hexadecanediol (97%), hexadecylamine (70%), iron(III) acetylacetonate ($Fe(acac)_3$), and manganese(II) acetylacetonate ($Mn(acac)_2$) were purchased from Aldrich Chemical Co.; ammonium fluoride (40% NH_4F), hydrogen peroxide (30% H_2O_2), and sulfuric acid (96% H_2SO_4) were from Mallinckrodt, EMD Chemicals Inc., and Riedel-deHaën, respectively. 16-Heptadecenoic acid was synthesized according to a modification of a method available in the literature (38, 39) (see the Supporting Information). Silicon(111) wafers (p-type) were obtained from North East Silicon Technologies Inc.

Synthesis of ω-Alkene-Terminated $MnFe_2O_4$ Nanoparticles. Using an approach modified from the literature (14−16), we prepared ω-alkene-terminated $MnFe_2O_4$ NPs via the thermal decomposition of organometallic precursors in the presence of 16-heptadecenoic acid with hexadecylamine and 1,2-hexadecanediol as stabilizing agents. The indicated portions of $Mn(acac)_2$ (0.05 g, 0.2 mmol), $Fe(acac)_3$ (0.14 g, 0.40 mmol), 1,2-hexadecanediol (0.52 g, 2.0 mmol), 16-heptadecenoic acid (0.32 g, 1.2 mmol), hexadecylamine (0.29 g, 1.2 mmol), and benzyl ether (6 mL) were mixed and stirred under argon in a 100 mL three-necked flask. The mixture was heated to 110 °C for a period of 1 h. For the 11.1 ± 1.4 nm $MnFe_2O_4$ NPs, the temperature of the reaction mixture was raised to 210 °C at a heating rate of 5 °C/min, and this temperature was maintained for 1 h. Using the same heating rate, we then increased the temperature to 285 °C for 1 h. After the solution was cooled, absolute ethanol (30 mL) was added into the crude solution of vinyl-terminated magnetite NPs. A black precipitate was isolated by centrifugation (30 min, 3000 rpm). Several post-preparative steps were performed to remove excess stabilizer. The precipitated nanoparticles were dissolved in toluene and stored in the refrigerator. For the 5.9 ± 1.1 nm $MnFe_2O_4$ NPs, which were prepared under identical conditions, an increase in the ramping of the temperature to 15 °C/min led to the smaller NP size.

Monolayer Preparation. Hydrogen-terminated silicon(111) surfaces were prepared following a known method (28, 40). The wafers were first cleaned in a hot "piranha solution", a mixture of 7:3 H_2SO_4(96%)/H_2O_2(30%), for 30 min (**CAUTION**: *"piranha solution" violently reacted with organic materials and should be handled carefully*), followed by rinsing with copious amounts of deionized Milli-Q water. During the same time frame, a 40% NH_4F solution was deoxygenated by bubbling argon. The freshly prepared wafer was etched in the deoxygenated 40% NH_4F solution for 10 min under a flow of argon, and rinsed with deionized Milli-Q water. Immediately after exposure, the wafers were dried with argon. The hydrogen-terminated silicon wafer and Schlenk flask containing the deoxygenated nonpolar solution with the vinyl-terminated $MnFe_2O_4$ nanoparticles were transferred into an inert-atmosphere glovebox. The nanoparticle solution was placed on the hydrogen-terminated silicon wafer, followed by evaporation of the nonpolar solution. With the NPs placed on the substrate, the wafer was exposed to a 254 nm UV lamp for 2 h in the glovebox. To physically remove any unbound NPs, the wafer was washed with toluene and EtOH under sonication for 10 min (21, 22, 41). As a final step, the wafer was dried at room temperature under a stream of argon before characterization.

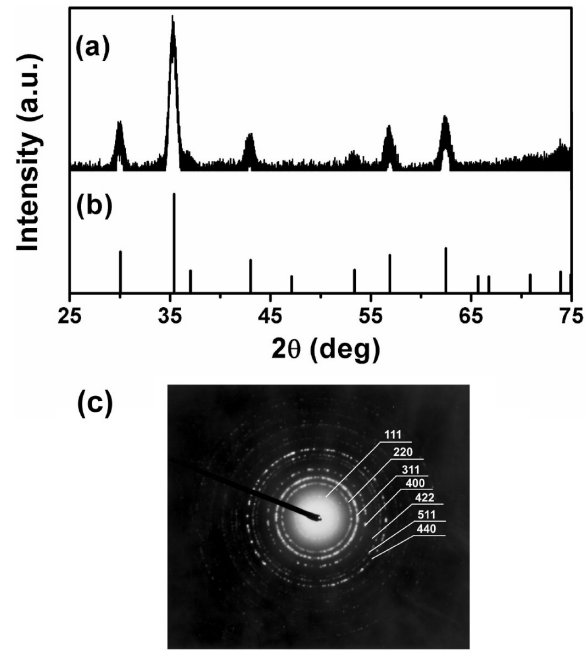

FIGURE 1. (a) X-ray diffraction patterns of $MnFe_2O_4$ NPs having an XRD-estimated average grain size of 10.6 nm at room temperature, (b) the JCPDS card data of $MnFe_2O_4$ (No. 10−0319), and (c) selected-area electron diffraction (SAED) of $MnFe_2O_4$ NPs.

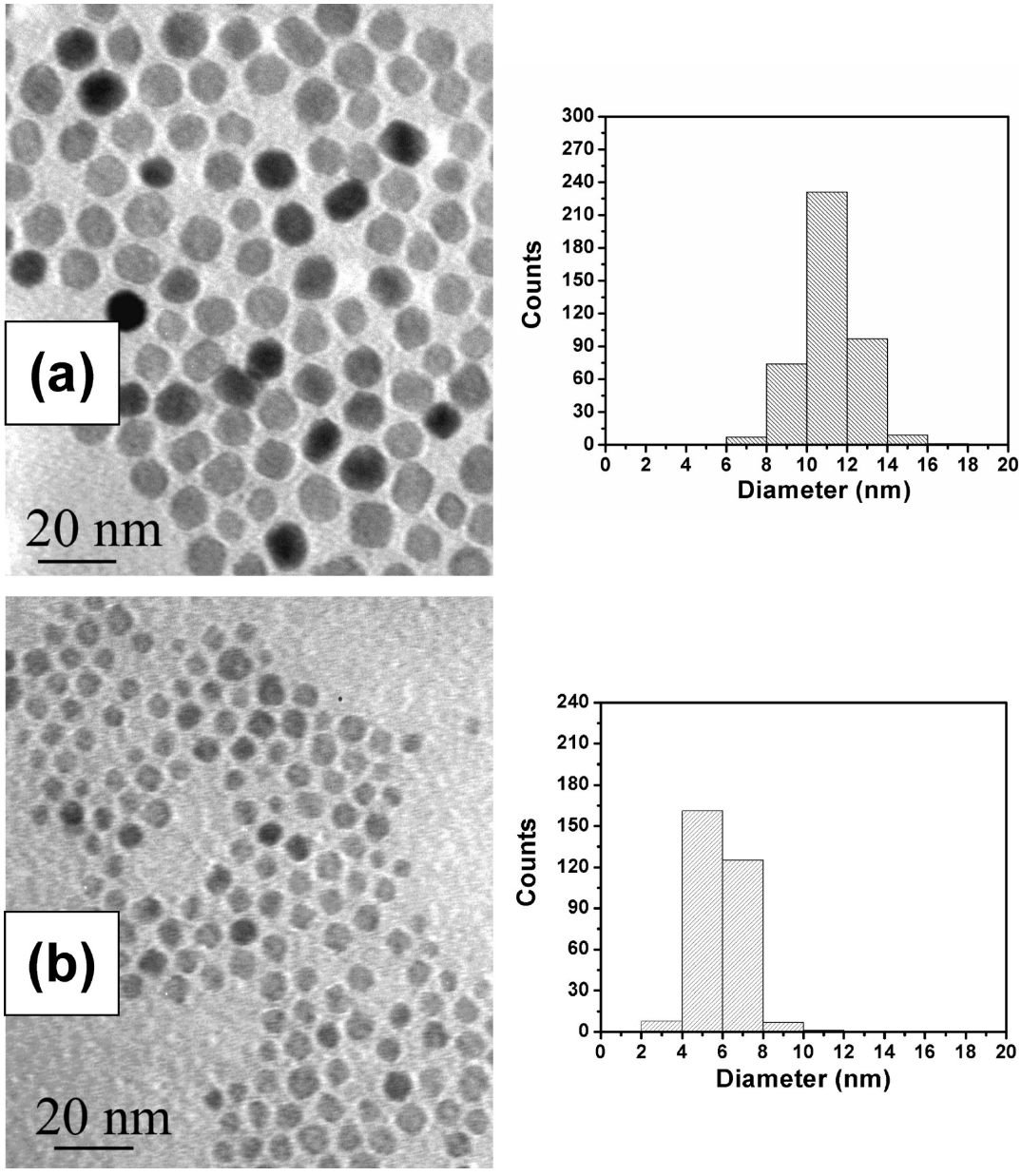

FIGURE 2. TEM bright-field images and size distributions of $MnFe_2O_4$ NPs having a size of (a) 11.1 ± 1.4 nm and (b) 5.9 ± 1.1 nm deposited from toluene on a carbon-coated copper grid and dried at room temperature.

Instrumentation. A JEOL 2000 FX electron microscope operating at an accelerating voltage of 200 kV was used to monitor the morphology and diffraction patterns of the $MnFe_2O_4$ NPs. All samples were prepared on carbon-coated TEM copper grids by the deposition of the NP solution on the surface, which was then allowed to dry completely at rt before being examined. Analysis by XRD was performed using a Siemens D5000 diffractometer with monochromatic Cu Kα radiation (λ = 1.540562 Å) to elucidate the nature of the powder. A step size of 0.02° and counting time of 30 s was used within the range of 25° ≤ 2θ ≤ 75° of step scanning at rt. FT-IR spectroscopy data were collected using a Galaxy series FTIR 5000 spectrometer. The spectra were collected for 64 scans at a resolution of 4 cm^{-1} and measured in the range of 4000−450 cm^{-1}. A SEM instrument (LEO scanning electron microscope) was used to observe the morphology and distribution of the NPs on the silicon wafer after immobilization of the NPs under UV irradiation. This instrument was operated at an accelerating voltage of 15 kV, and no additional conductive layers were coated on the samples. XPS spectra of the surface of the silicon wafer were collected using a PHI 5700 X-ray photoelectron spectrometer (XPS) equipped with a monochromatic Al Kα X-ray source ($h\nu$ = 1486.7 eV) at 90° relative to the axis of a hemispherical energy analyzer. The spectrometer was configured to operate at high resolution with a pass energy of 23.5 eV, a photoelectron takeoff angle of 45° from the surface, and an analyzer spot diameter of 2 mm. Spectra were collected at rt, and the base pressure in the chamber during operation of the instrument was 3 × 10^{-9} Torr. Twenty scans each were accumulated to obtain the Fe(2p) and Mn(2p) spectra. All peaks were quantified by curve-fitting software with respect to spin−orbit splitting. Magnetic measurements with a magnetic field up to 5 T and a temperature ranging between 5 and 225 K were performed using a Quantum Design superconducting quantum interference device (SQUID) MPMS magnetometer.

RESULTS AND DISCUSSION

Oleic acid and oleylamine are commonly used in the preparation of monodisperse magnetic nanoparticles be-

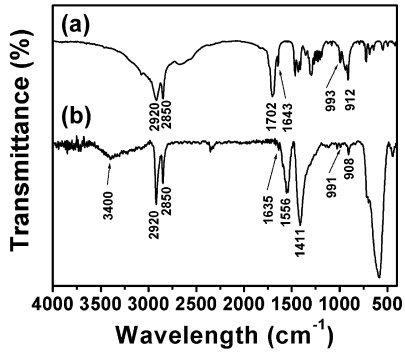

FIGURE 3. FTIR spectra of (a) pure 16-heptadecenoic acid and (b) surfactant-modified $MnFe_2O_4$ NPs.

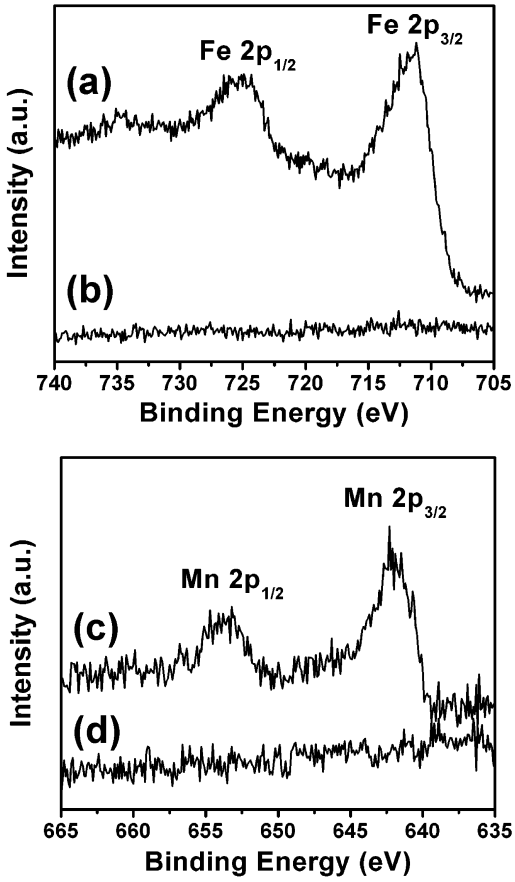

FIGURE 4. XPS spectra of covalently attached 11.1 ± 1.4 nm NPs on a silicon(111) wafer (a) Fe 2P with UV, (b) Fe 2P without UV, (c) Mn 2P with UV, and (d) Mn 2P without UV irradiation, after washing separately with toluene and ethanol under sonication.

cause the presence of both species leads to surfactant-stabilized nanoparticles with narrow size distributions (14). Given this background and numerous trials (37), we synthesized 16-heptadecenoic acid for use as a cosurfactant to prepare ω-alkene-terminated $MnFe_2O_4$ NPs (as described in the Experimental Section), where the carboxylate moieties were designed to bind to the surface of the magnetic NPs (9, 21, 37, 42), and the terminal double bonds were designed to anchor covalently the NPs on hydrogen-terminated silicon via hydrosilylation (37, 43).

Characterization of ω-Alkene-Terminated $MnFe_2O_4$ NPs. Figure 1 shows X-ray diffraction patterns and selected area electron diffraction (SAED) of freshly synthesized ω-alkene-terminated $MnFe_2O_4$ NPs. The observed diffraction peaks and rings of the vinyl-functionalized NPs matched well with the known characteristic peaks and the ring spacing for the diffraction pattern of $MnFe_2O_4$ (JCPDS card number 10−0319). The width of the diffraction peaks can be used to estimate the particle size (44); accordingly, analysis using Scherrer's equation reveals that the 5 °C/min heating rate gave $MnFe_2O_4$ NPs with an average grain size of 10.6 nm (see Figure 1). In contrast, the 15 °C/min heating rate gave $MnFe_2O_4$ NPs with an XRD-determined average grain size of 6.5 nm (see Figure S1 in the Supporting Information).

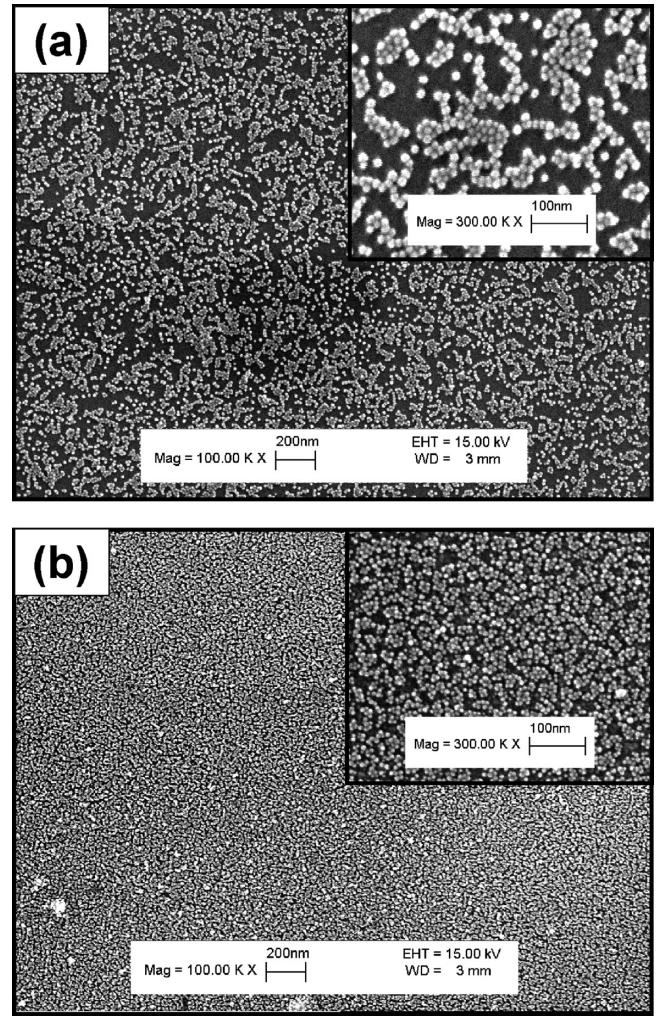

FIGURE 5. SEM images of covalently bound vinyl-terminated $MnFe_2O_4$ NPs having a size of (a) 11.1 ± 1.4 nm and (b) 5.9 ± 1.1 nm on Si wafers after UV treatment.

The size and morphology of the $MnFe_2O_4$ NPs was further characterized by TEM (Figure 2). Analysis by TEM of the products of the different heating rates revealed that these spherical particles have an average size of 11.1 ± 1.4 nm for 5 °C/min and 5.9 ± 1.1 nm for 15 °C/min; these values are consistent with the average grain sizes estimated above by XRD (10.6 and 6.5 nm, respectively). We recently demonstrated that a heating rate of 10 °C/min in reaction of $Fe(acac)_3$ and $Mn(acac)_2$ with long chain surfactants in a benzyl ether gave monodisperse $MnFe_2O_4$ NPs with a size of 8.6 ± 1.4 nm (37). As such, the trend in the heating rate appears to be highly systematic, where an increase in the

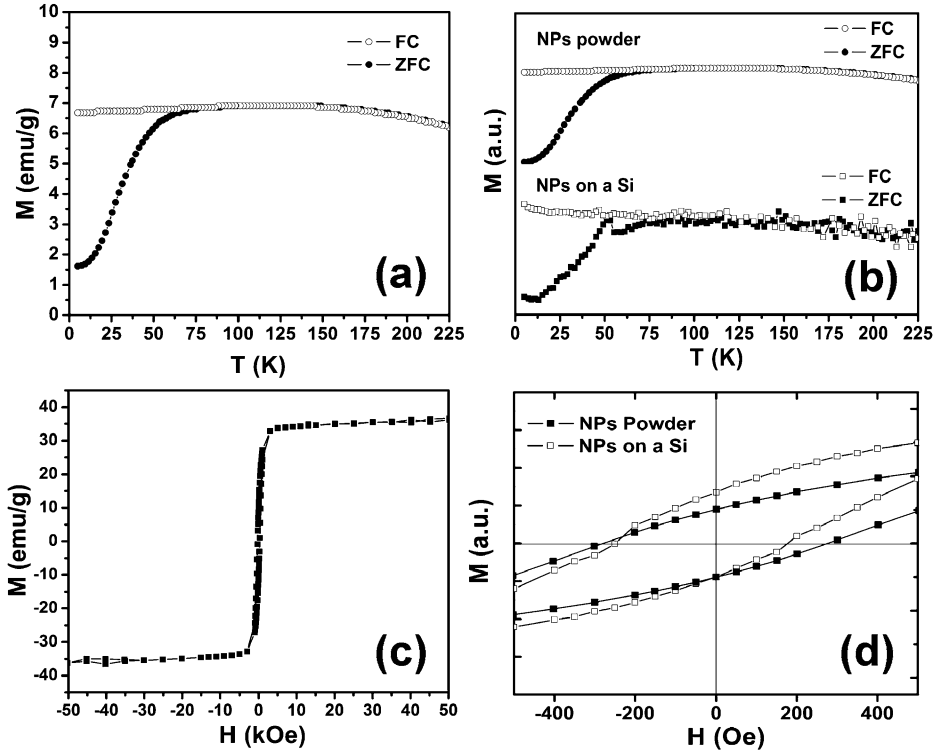

FIGURE 6. Magnetization measurements for the 11.1 ± 1.4 nm $MnFe_2O_4$ NPs: (a) zero-field-cooled (filled symbols) and field-cooled (open symbols) magnetization of the NP powder at a field of 100 Oe, (b) comparison of NP powder and NPs anchored on a Si wafer, (c) magnetization curve of the NP powder at 5 K, and (d) enlarged magnetization hysteresis loop behavior of the NP powder (filled symbols) and NPs anchored on a Si wafer (open symbols).

rate of heating leads to smaller particles: 11.1 ± 1.4 nm (5 °C min), 8.6 ± 1.4 nm (10 °C/min), and 5.9 ± 1.1 nm (15 °C/min). Similarly, as the rate of heating was increased during the synthesis of FePt NPs, the average size of the NPs was observed to decrease; this phenomenon was interpreted to reflect enhanced particle nucleation at faster heating rates, which leads to greater numbers of nuclei during the initial stages of particle growth (45, 46). It is likely that the same phenomenon is at work here, where our custom-designed surfactant system permits the size-selective synthesis of $MnFe_2O_4$ NPs in a precisely tunable fashion simply by adjusting the rate of heating.

When the NPs were deposited on the carbon-coated copper grid, they formed a monolayer in which the individual NPs exhibited little or no aggregation (see Figure 2). The presence of the organic ligands appears to prevent the particle aggregation during monolayer formation. This observation is consistent with previous work that determined that $MnFe_2O_4$ NPs can be stabilized by oleic acid and oleylamine in the presence of 1,2-alkanediols (14).

Figure 3a shows an FTIR spectrum of the custom-designed surfactant 16-heptadecenoic acid. The strong band at 1702 cm^{-1} can be assigned to the carbonyl stretching vibration. This band, however, disappears in the FTIR spectrum of the $MnFe_2O_4$ NPs, while new strong peaks appear at 1556 and 1411 cm^{-1} (Figure 3b), which can be assigned to the antisymmetric and symmetric vibrations of the carboxylate anions, $\nu_{as}COO^-$ and ν_sCOO^-, respectively (47−49). These changes indicate that most of the carboxylic acid moieties are bound to the $MnFe_2O_4$ NPs, given that the ligands are chemically bound to the NP surface through the bidentate COO^- headgroup (20). The spectrum of the C═C terminal group for the unbound carboxylic acid shows bands at 1643, 993, and 912 cm^{-1}, which can be assigned to C═C stretching, C═C out-of-plane deformation, and the $=CH_2$ wagging mode (50). For the ligand moieties bound to the $MnFe_2O_4$ nanoparticles, these three bands are still present, but shift slightly to 1635, 991, and 908 cm^{-1}, respectively. This shift probably reflects differences in conformation/packing for the free vs bound ligand molecules. We note also that the presence of the broad band at ~3400 cm^{-1} indicates that the hydroxyl moieties of 1,2-hexadecanediol and the amino groups of hexadecylamine are also bound to the surface of the nanoparticles (37).

Anchoring the $MnFe_2O_4$ NPs to the Surface of Silicon. The $MnFe_2O_4$ NPs were anchored to hydrogen-terminated silicon via UV-induced hydrosilylation (37, 51). The resulting surface was characterized by XPS and SEM after sonicating the silicon wafers in a nonpolar solvent (toluene) and a polar solvent (ethanol) for 10 min each.

Analysis by XPS confirmed the presence of the $MnFe_2O_4$ NPs on the silicon surface (Figure 4). The Fe 2P and Mn 2P spectra in a and c in Figure 4 show well-defined peaks that are consistent with $MnFe_2O_4$ NPs, where the Fe ($2P_{3/2}$) and Fe ($2P_{1/2}$) signals are centered at 711.0 and 724.8 eV in the XPS spectra, respectively, and the Mn ($2P_{3/2}$) and Mn ($2P_{1/2}$) are centered at 641.3 and 654.1 eV, respectively (37, 52). In contrast, the Fe 2P and Mn 2P spectra in b and d in Figure 4 show no peaks for Mn or Fe. These samples were not

exposed to UV radiation; consequently, the sonication steps were able to remove the nonanchored nanoparticles from the surface. These data provide firm support for our claim that UV treatment leads to the covalent binding of the ω-alkene-modified $MnFe_2O_4$ NPs (41).

The large-area SEM images in Figure 5 illustrate the coverage of two different sizes of the spherical $MnFe_2O_4$ NPs on the silicon substrate. These images suggest that the degree of coverage (or packing density) is greater for the smaller NPs. It is plausible that the washing/sonication steps are more detrimental to the binding of the larger NPs because greater masses and stresses are involved. Additional studies are currently under way to obtain a better understanding of the impact of size on coverage/organization of the deposited NPs.

Magnetic Properties. To study the magnetic properties of the 11.1 ± 1.4 nm $MnFe_2O_4$ NPs in the solid state and on silicon substrates, we used a SQUID magnetometer to perform zero-field-cooling (ZFC) and field-cooling (FC) and field-dependent magnetization measurements. The behavior of the temperature-dependent magnetization from 5 to 225 K was measured in an applied field of 100 Oe. Panels a and b in Figure 6 show ZFC/FC curves of the $MnFe_2O_4$ NP powder and a comparison of both the NP powder and surface-bound NPs. The observed maximum temperature (T_{max}) value on the ZFC curve, in general, relates to the average blocking temperature at which the time scale of the experiment equals the relaxation time of the magnetic moment (53). The broad T_{max} of the $MnFe_2O_4$ NP powder at ~90 K is similar to that of the ones covalently attached to the surface of silicon. The comparison confirms that the ω-alkene-terminated $MnFe_2O_4$ NPs are effectively bound to the silicon substrate and that their magnetic properties are not significantly affected by being bound to that substrate. We note that a magnetic anomaly at ~53 K observed on the ZFC curve of measured NPs attached to the silicon wafer can be attributed to the magnetic ordering of a small amount of oxygen in the sample chamber. This effect is discernible when the sample's own magnetization is in the range of 1×10^{-5} emu or lower (54).

Figure 6c shows the $M(H)$ hysteric magnetization behavior at 5 K for the $MnFe_2O_4$ NP powder. The magnetization saturation of the $MnFe_2O_4$ NP powder is ~36 emu/g, which is much lower than the reported bulk value of 110 emu/g (55). Such a strong decrease might be due to surface spin-canting effects caused by a nonmagnetic layer of surfactants at the particle surface (55–57). Separately, Figure 6d shows a small distinctive difference in coercivity (H_c) between the two samples. In the case of the surface-bound NPs, the range of coercivity for the hysteresis loop is smaller than that for the NP powder. The smaller range might be due to the surface state of the particles or perhaps different dipolar interparticle interactions for the surface-bound NPs when compared to the NP powder. Additionally, Figure 6d shows slightly asymmetric magnetization curves for the surface-bound NPs. The asymmetry might arise from the surface states of the NPs in the presence of several magnetic phases

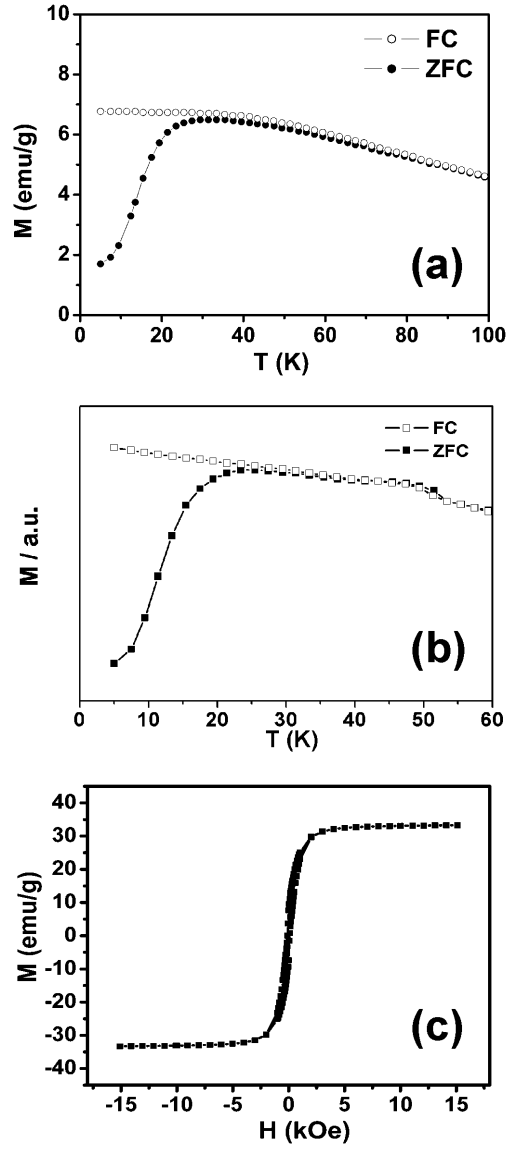

FIGURE 7. Magnetization measurements for the 5.9 ± 1.1 nm $MnFe_2O_4$ NPs: zero-field-cooled (filled symbols) and field-cooled (open symbols) magnetization of (a) the NP powder at a field of 100 Oe and (b) the NPs anchored on a Si wafers at a field of 100 Oe, and (c) magnetization curve of the NP powder at 5 K.

with different magnetic anisotropy energies. Magnetic inhomogenetity of individual surface-bound NPs on Si could give rise to an exchange bias effect (58).

Interestingly, as the size of $MnFe_2O_4$ NP changes from 11.1 ± 1.4 nm to 5.9 ± 1.1 nm, the blocking temperature as measured for the powder decreases from ~90 to ~35 K, and also the saturation magnetization drops from ~36 to ~33 emu/g. (see Figure 7a). This type of size-dependence of the magnetic properties is similar to that found in previous work (56, 59, 60). On the basis of the Stoner–Wohlfarth theory, the magnetic anisotropy energy of a nanoparticle increases proportionally to the volume of a nanoparticle (61). Magnetic anisotropy energy is an energy barrier for blocking the superparamagneticity of nanoparticles. To overcome this energy barrier with thermal energy, one needs to exceed a threshold temperature called the blocking temperature. Therefore, the blocking temperature depends on the size of

the nanoparticles (62). The saturation magnetization slightly decreases with the decreasing size of the nanoparticles due to the proportionately increasing volume and to its dependence upon the existence of the pinned magnetic moments at the surface of the nanoparticles (56).

Finally, the observed blocking temperature of the 5.9 ± 1.1 nm surface-bound $MnFe_2O_4$ NPs was similar to the measurement obtained for the corresponding $MnFe_2O_4$ powder (see Figure 7b). Our attempts, however, to measure the $M(H)$ hysteric magnetization behavior of the 5.9 ± 1.1 nm immobilized NPs were unsuccessful.

CONCLUSIONS

Monodisperse $MnFe_2O_4$ NPs functionalized with a terminally unsaturated surfactant under thermal decomposition reaction conditions were successfully prepared. Transmission electron microscopy (TEM), Fourier-transform infrared (FT-IR) spectroscopy, and X-ray diffraction (XRD) measurements were used to characterize the size, morphology, and composition of the nanoparticles. From these studies, we concluded that the size of these NPs can be precisely tuned simply by adjusting the heating rate, with all other reaction conditions being constant. These size-controlled NPs were covalently anchored on a hydrogen-terminated silicon(111) substrate, which led to the formation of covalently bound monolayer arrays. These findings provide a starting point for the fabrication of stable patterned magnetic NP arrays via the use of standard photolithographic mask-based patterning, making it possible to create bit-patterned ultrahigh density magnetic recording media and nanoscale biomagnetic sensors.

Acknowledgment. The National Science Foundation (ECCS-0926027) and the state of Texas through the Texas Center for Superconductivity provided generous support for this research.

Supporting Information Available: A detailed description of the preparation of 16-heptadecenoic acid along with XRD data for the 5.9 ± 1.1 nm ω-alkene-terminated $MnFe_2O_4$ NPs (PDF). This material is available free of charge via the Internet at http://pubs.acs.org.

REFERENCES AND NOTES

(1) Weller, D.; Moser, A.; Folks, L.; Best, M. E.; Lee, W.; Toney, M. F.; Schwickert, M.; Thiele, J.-U.; Doerner, M. F. *IEEE Trans. Magn.* **2000**, *36*, 10.
(2) Sun, S. H.; Murray, C. B.; Weller, D.; Folks, L.; Moser, A. *Science* **2000**, *287*, 1989.
(3) Speliotis, D. E. *J. Magn. Magn. Mater.* **1999**, *193*, 29.
(4) Weller, D.; Moser, A. *IEEE Trans. Magn.* **1999**, *35*, 4423.
(5) Cornell, R. M.; Schwertmann, U. *The Iron Oxide-Structure, Properties, Reactions, Occurrence and Uses*; VCH: Weinheim, Germany, 1996.
(6) Bonnemain, B. *J. Drug Targeting* **1998**, *6*, 167.
(7) Torchilin, V. P. *Eur. J. Pharm. Sci.* **2000**, *11*, S81.
(8) Gupta, P. K.; Hung, C. T.; Lam, F. C.; Perrier, D. G. *Int. J. Pharm.* **1988**, *43*, 167.
(9) Song, H.-T.; Choi, J.-s.; Huh, Y.-M.; Kim, S.; Jun, Y.-w.; Suh, J.-S.; Cheon, J. *J. Am. Chem. Soc.* **2005**, *127*, 9992.
(10) Tromsdorf, U. I.; Bigall, N. C.; Kaul, M. G.; Bruns, O. T.; Nikolic, M. S.; Mollwitz, B.; Sperling, R. A.; Reimer, R.; Hohenberg, H.; Parak, W. J.; Forster, S.; Beisiegel, U.; Adam, G.; Weller, H. *Nano Lett.* **2007**, *7*, 2422.
(11) Willard, M. A.; Kurihara, L. K.; Carpenter, E. E.; Calvin, S.; Harris, V. G. *Int. Mater. Rev.* **2004**, *49*, 125.
(12) Moumen, N.; Pileni, M. P. *J. Phys. Chem.* **1996**, *100*, 1867.
(13) Liu, C.; Zou, B.; Rondinone, A. J.; Zhang, Z. J. *J. Phys. Chem. B.* **2000**, *104*, 1141.
(14) Sun, S.; Zeng, H.; Robinson, D. B.; Raoux, S.; Rice, P. M.; Wang, S. X.; Li, G. *J. Am. Chem. Soc.* **2004**, *126*, 273.
(15) Zeng, H.; Rice, P. M.; Wang, S. X.; Sun, S. *J. Am. Chem. Soc.* **2004**, *126*, 11458.
(16) Leem, G.; Sarangi, S.; Zhang, S.; Rusakova, I.; Brazdeikis, A.; Litvinov, D.; Lee, T. R. *Cryst. Growth Des.* **2009**, *9*, 32.
(17) Tang, Z. X.; Chen, J. P.; Sorensen, C. M.; Klabunde, K. J.; Hadjipanayis, G. C. *Phys. Rev. Lett.* **1992**, *68*, 3114.
(18) Burda, C.; Chen, X.; Narayanan, R.; El-Sayed, M. A. *Chem. Rev.* **2005**, *105*, 1025.
(19) Murray, C. B.; Kagan, C. R.; Bawendi, M. G. *Annu. Rev. Mater. Sci.* **2000**, *30*, 545.
(20) Fanizza, E.; Cozzoli, P. D.; Curri, M. L.; Striccoli, M.; Sardella, E.; Agostiano, A. *Adv. Funct. Mater.* **2007**, *17*, 201.
(21) Cattaruzza, F.; Fiorani, D.; Flamini, A.; Imperatori, P.; Scavia, G.; Suber, L.; Testa, A. M.; Mezzi, A.; Ausanio, G.; Plunkett, W. R. *Chem. Mater.* **2005**, *17*, 3311.
(22) Altavilla, C.; Ciliberto, E.; Gatteschi, D.; Sangregorio, C. *Adv. Mater.* **2005**, *17*, 1084.
(23) Buriak, J. M.; Stewart, M. P.; Geders, T. W.; Allen, M. J.; Choi, H. C.; Smith, J.; Raftery, D.; Canham, L. T. *J. Am. Chem. Soc.* **1999**, *121*, 11491.
(24) Schmeltzer, J. M.; Porter, L. A., Jr.; Stewart, M. P.; Buriak, J. M. *Langmuir* **2002**, *18*, 2971.
(25) Cicero, R. L.; Linford, M. R.; Chidsey, C. E. D. *Langmuir* **2000**, *16*, 5688.
(26) Effenberger, F.; Götz, G.; Bidlingmaier, B.; Wezstein, M. *Angew. Chem., Int. Ed.* **1998**, *37*, 2462.
(27) Strother, T.; Cai, W.; Zhao, X.; Hamers, R. J.; Smith, L. M. *J. Am. Chem. Soc.* **2000**, *122*, 1205.
(28) Asanuma, H.; Lopinski, G. P.; Yu, H.-Z. *Langmuir* **2005**, *21*, 5013.
(29) de Smet, L. C. P. M.; Stork, G. A.; Hurenkamp, G. H. F.; Sun, Q.-Y.; Topal, H.; Vronen, P. J. E.; Sieval, A. B.; Wright, A.; Visser, G. M.; Zuilhof, H.; Sudhölter, E. J. R. *J. Am. Chem. Soc.* **2003**, *125*, 13916.
(30) Sun, Q.-Y.; de Smet, L. C. P. M.; van Lagen, B.; Giesbers, M.; Thune, P. C.; van Engelenburg, J.; de Wolf, F. A.; Zuilhof, H.; Sudholter, E. J. R. *J. Am. Chem. Soc.* **2005**, *127*, 2514.
(31) Webb, L. J.; Lewis, N. S. *J. Phys. Chem. B.* **2003**, *107*, 5404.
(32) Boukherroub, R.; Morin, S.; Bensebaa, F.; Wayner, D. D. M. *Langmuir* **1999**, *15*, 3831.
(33) de Villeneuve, C. H.; Pinson, J.; Bernard, M. C.; Allongue, P. *J. Phys. Chem. B.* **1997**, *101*, 2415.
(34) Wagner, P.; Nock, S.; Spudich, J. A.; Volkmuth, W. D.; Chu, S.; Cicero, R. L.; Wade, C. P.; Linford, M. R.; Chidsey, C. E. D. *J. Struct. Biol.* **1997**, *119*, 189.
(35) Linford, M. R.; Fenter, P.; Eisenberger, P. M.; Chidsey, C. E. D. *J. Am. Chem. Soc.* **1995**, *117*, 3145.
(36) Lasseter, T. L.; Clare, B. H.; Abbott, N. L.; Hamers, R. J. *J. Am. Chem. Soc.* **2004**, *126*, 10220.
(37) Leem, G.; Jamison, A. C.; Zhang, S.; Litvinov, D.; Lee, T. R. *Chem. Commun.* **2008**, 4989.
(38) Vallant, T.; Kattner, J.; Brunner, H.; Mayer, U.; Hoffmann, H. *Langmuir* **1999**, *15*, 5339.
(39) Effenberger, F.; Heid, S. *Synthesis* **1995**, *9*, 1126.
(40) Mengistu, T. Z.; Goel, V.; Horton, J. H.; Morin, S. *Langmuir* **2006**, *22*, 5301.
(41) Yamanoi, Y.; Shirahata, N.; Yonezawa, T.; Terasaki, N.; Yamamoto, N.; Matsui, Y.; Nishio, K.; Masuda, H.; Ikuhara, Y.; Nishihara, H. *Chem.—Eur. J.* **2006**, *12*, 314.
(42) Boal, A. K.; Das, K.; Gray, M.; Rotello, V. M. *Chem. Mater.* **2002**, *14*, 2628.
(43) Faucheux, A.; Gouget-Laemmel, A. C.; Henry de Villeneuve, C.; Boukherroub, R.; Ozanam, F.; Allongue, P.; Chazalviel, J.-N. *Langmuir* **2006**, *22*, 153.
(44) Klug, H. P.; Alexander, L. E. *X-Ray Diffraction Procedure*, 2nd ed.; Wiley, New York, 1974.
(45) Chen, M.; Liu, J. P.; Sun, S. *J. Am. Chem. Soc.* **2004**, *126*, 8394.
(46) Nandwana, V.; Elkins, K. E.; Poudyal, N.; Chaubey, G. S.; Yano, K.; Liu, J. P. *J. Phys. Chem. C.* **2007**, *111*, 4185.
(47) Shukla, N.; Liu, C.; Jones, P. M.; Weller, D. *J. Magn. Magn. Mater.* **2003**, *266*, 178.

(48) Vestal, C. R.; Zhang, Z. J. *J. Am. Chem. Soc.* **2003**, *125*, 9828.
(49) Samia, A. C. S.; Schlueter, J. A.; Jiang, J. S.; Bader, S. D.; Qin, C.-J.; Lin, X.-M. *Chem. Mater.* **2006**, *18*, 5203.
(50) Fiegland, L. R.; Fleur, M. M. S.; Morris, J. R. *Langmuir* **2005**, *21*, 2660.
(51) Cai, W.; Peck, J. R.; van der Weide, D. W.; Hamers, R. J. *Biosens. Bioelectron.* **2004**, *19*, 1013.
(52) Hu, J.; Lo, I. M. C.; Chen, G. *Langmuir* **2005**, *21*, 11173.
(53) Si, S.; Li, C.; Wang, X.; Yu, D.; Peng, Q.; Li, Y. *Cryst. Growth Des.* **2005**, *5*, 391.
(54) Dubroca, T.; Hack, J.; Hummel, R. *Phys. Rev. B* **2006**, *74*, 026403.
(55) Balaji, G.; Gajbhiye, N. S.; Wilde, G.; Weissmüller, J. *J. Magn. Magn. Mater.* **2002**, *242−245*, 617.
(56) Aslam, M.; Schultz, E. A.; Sun, T.; Meade, T.; Dravid, V. P. *Cryst. Growth Des.* **2007**, *7*, 471.
(57) Daou, T. J.; Grenèche, J. M.; Pourroy, G.; Buathong, S.; Derory, A.; Ulhaq-Bouillet, C.; Donnio, B.; Guillon, D.; Begin-Colin, S. *Chem. Mater.* **2008**, *20*, 5869.
(58) Shavel, A.; Rodrguez-Gonzlez, B.; Pacifico, J.; Spasova, M.; Farle, M.; Liz-Marzn, L. M. *Chem. Mater.* **2009**, *21*, 1326.
(59) Masala, O.; Seshadri, R. *Chem. Phys. Lett.* **2005**, *402*, 160.
(60) Song, Q.; Ding, Y.; Wang, Z. L.; Zhang, J. *Chem. Mater.* **2007**, *19*, 4633.
(61) Stoner, E. C.; Wohlfarth, E. P. *IEEE Trans. Magn.* **1991**, *27*, 3475.
(62) Lu, A.-H.; Salabas, E. L.; Schüth, F. *Angew. Chem., Int. Ed.* **2007**, *46*, 1222.

AM100457V